ORIGINAL ARTICLE

Investigation the changes in the concentration of dye organic pollutant using magnetic titania nanoparticles incorporated on surface of graphene oxide

Sedigheh Abbasi[1] 🄳

Abstract

In this study, in order to prepare magnetic nanocomposite, TiO_2 nanoparticles and Fe_3O_4 nanoparticles are uniformly synthesized on the surface of graphene oxide by hydrolysis and hydrothermal methods, respectively. The efficiency of the synthesized nanocomposite (MGO@ Fe_3O_4) for the photocatalytic decomposition of methyl orange is investigated and compared with the magnetic hybrid without graphene oxide (Fe_3O_4@ TiO_2). FTIR and VSM analysis are used to characterize the synthesized nanocomposite and hybrid. FTIR analysis confirmed the bond vibrations in TiO_2 and Fe_3O_4 molecules present in both photocatalytic samples. VSM analysis shows the superparamagnetic properties of the synthesized photocatalysts. Investigating the effect of irradiation time and photocatalyst concentration on the ability to remove methyl orange by magnetic photocatalysts showed that both parameters have a positive effect, although based on the results of statistical analysis, irradiation time is more effective than photocatalyst concentration. It is also observed that despite the independent operating parameters having a significant effect on the photocatalytic activity of nanocomposite and hybrid, the mutual interaction between individual factors in nanocomposite and hybrid behaves differently.

Keywords Graphene oxide · Magnetic photocatalysts · Mutual interaction · Organic pollutants · Statistical analysis

Introduction

Due to the growth of human societies and the development of various industries, including chemical and textile industries, human health and the environment are under serious threat. This is due to the release of wastewater from such industries into water systems (Abbasi 2018, 2019). The presence of toxic pollutants such as dyes can be one of the effective factors in the occurrence of cancer in humans. Therefore, one of the most important duties of humans to preserve the health of the environment is to prevent the discharge of wastewater into water systems and also to reduce the amount of pollution in the wastewater of such industries (Ghaderi et al. 2018; Yuan et al. 2012). So far, several methods have been investigated to reduce the amount of wastewater pollution, which can be mentioned as membrane filtration, ion exchange, adsorption, and advanced oxidation process (AOP) (Abbasi 2020; Zhu et al. 2015). In recent years, the advanced oxidation method has attracted the attention of researchers due to its cost-effectiveness and easy application as one of the widely used methods to remove dye organic pollutants. The advanced oxidation method is based on the use of a semiconductor as a photocatalyst. The semiconductor used must have the ability to be excited and also produce electron–hole pairs in the valence layer and the conduction layer, respectively (Abbasi and Hasanpour 2017; Kim et al. 2015). The most commonly used photocatalysts are ZnO and TiO_2. One of the effective factors in choosing the photocatalyst is the stability of the produced electric charges. Considering that the recombination rate of generated electron–hole pairs in oxide semiconductors is very fast, therefore, its stability decreases significantly (Gao and Sun 2014; Reddy et al. 2015). Therefore, one of the recent challenges is the use of techniques to increase the stability of load carriers. Connecting semiconductor photocatalysts on the surface of materials with a porous structure that have a high surface-to-volume ratio, significant electron transfer speed, and high absorption ability is one of the effective methods to increase

✉ Sedigheh Abbasi
s.abbasi@esfarayen.ac.ir; abasi_1362@yahoo.com

1 Central Research Laboratory, Esfarayen University of Technology, Esfarayen, North Khorasan, Iran

the stability of produced electron–hole pairs and photocatalytic activity (Abbasi et al. 2017a, b; Abdel-Messih et al. 2013). Due to the honeycomb structure as well as unique properties, graphene oxide (GO) has been considered as a potential candidate for the basis of semiconductor photocatalysts (Fan et al. 2021; Gan et al. 2018; Tao et al. 2023). Despite the fact that the use of graphene oxide increases the speed of electron transfer, improves the stability of electron–hole pairs, and increases the decomposition rate of organic pollutants, the separation of photocatalysts, including photocatalysts based on carbon materials, from aqueous suspensions is very complicated and difficult. Therefore, in order to overcome this problem and facilitate the separation process, the use of magnetic nanoparticles such as Fe_3O_4 in the photocatalyst structure is considered as an effective and practical method (Benjwal et al. 2015). The connection of Fe_3O_4 nanoparticles on the surface of graphene oxide causes the separation of graphite sheets and this prevents the accumulation of graphene oxide sheets. Therefore, the contact surface of the photocatalytic nanocomposite increases significantly. The presence of Fe_3O_4 nanoparticles in the structure of the photocatalyst reduces the cost of separation and also enables the reuse of the photocatalyst.

In this research, a new type of magnetic nanocomposite based on graphene oxide is synthesized so that TiO_2 photocatalytic nanoparticles and Fe_3O_4 magnetic nanoparticles are uniformly attached on the surface of graphene oxide which contains functional groups containing oxygen. The photocatalytic activity of the synthesized magnetic nanocomposite is studied to destruction of methyl orange (MO) as an organic dye pollutant.

Materials and methods

Synthesis of photocatalytic samples

The synthesis of magnetic nanocomposites based on graphene oxide includes several steps. In the first step, magnetic Fe_3O_4 nanoparticles should be synthesized uniformly on the surface of graphene oxide (Novin Nano Negasht Company, Iran). For this purpose, the method presented in the previous reports of this team is used (Abbasi 2021a, b; Abbasi et al. 2020). Briefly, a mixture of Ethylene glycol (EG, $C_2H_6O_2$, 99.9%) and graphene oxide with a unit weight ratio is used. The amount of ethylene glycol and graphene oxide used in this step is equal to 45 mg. In order to obtain a uniform mixture, it is mixed using an ultrasonic bath for 30 min. Next, 0.225 g of ferric acetylacetonate (Fe(acac)$_3$, Merck) is added to the homogenized suspension and placed in an ultrasonic bath for 30 min. Then, 1.5 g of ammonium acetate (NH$_4$Ac, NH$_4$CH$_3$CO$_2$, 99.9%) is added to the mixture and after 30 min of mixing; it is transferred to an autoclave. In

order to start the process of forming magnetic Fe_3O_4 nanoparticles on the surface of graphene oxide, the autoclave is transferred to an oven with a temperature of 200 °C for 24 h. After finishing the heating process inside the oven, the autoclave is removed from the oven to reach the ambient temperature. After opening the autoclave lid, the mixture inside is separated using a strong magnet and after washing the prepared magnetized graphene oxide (MGO) is dried at 60 °C for 12 h.

The second step includes the synthesis of photocatalytic TiO_2 nanoparticles on the surface of MGO. The hydrolysis method presented in previous reports (Abbasi et al. 2015) is used to synthesize TiO_2 photocatalytic nanoparticles on the surface of MGO. Therefore, 0.1 g of MGO prepared in the previous step is dispersed in 100 ml of distilled water and placed in an ultrasonic bath for 30 min to create a uniform mixture. In order to nucleate and synthesize TiO_2 nanoparticles, tetra chloride titanium (TiCl$_4$, 99%, Merck) is used as a precursor. Add 0.8 ml of the precursor drop by drop to the uniformed mixture on the magnetic stirrer. The mixing process is carried out for 5 h at ambient temperature, and then, the temperature is increased to 60 °C, and it is mixed at this temperature for 12 h. At the end, the processed mixture is filtered, washed and calcined for 3 h at 350 °C. The obtained sample is coded as MGO@TiO$_2$. The characterization of the synthesized samples is determined using Fourier transform infrared (FTIR, Tensor 70) and vibrating sample magnetometer (VSM, Meghnatis Daghigh Kavir Co., Iran). FTIR analysis has the ability to determine functional groups as well as vibrations between atoms. VSM analysis is also used to determine the magnetic properties of samples.

Photocatalytic decomposition of organic dye pollutant

The photocatalytic degradation of methyl orange as an organic pollutant using synthesized photocatalytic samples is investigated in a reactor equipped with a cooling system to reduce the temperature of the light source. The light source used to excite the electrons of the capacitance layer of photocatalysts is a medium pressure mercury vapor lamp. In the design of the used reactor, the light source should be placed exactly in the middle of the mixture containing the pollutant and photocatalyst so that the amount of radiation to the mixture is completely uniform. The concentration of methyl orange in all investigated effluents is equal to 10 ppm. While the concentration of synthesized photocatalysts in different experiments is variable and equal to 0.05%wt, 0.1%wt and 0.2%wt.

In each experiment, 80 ml of aqueous methyl orange solution with a concentration of 10 ppm is used, and the effect of the type and concentration of synthesized photocatalysts is investigated. The prepared suspensions

containing a certain concentration of each of the $Fe_3O_4@$ TiO_2 and MGO@TiO_2 magnetic photocatalysts are mixed for one hour in the reactor, whose light source is turned off, using an ultrasonic bath to establish the balance of absorption and desorption. Then, by draining 2 ml of the mixture and removing the photocatalysts inside it using a magnet, the amount of absorption of the pollutant is measured at wavelength of 464 nm using a spectrophotometer (Perkin Elmer Company). The recorded absorbance is considered as A_0. Next, the UV lamp inside the reactor is turned on and the suspension is irradiated. At time intervals of every 5 min, 2 ml of the suspension is drained and after separating of photocatalysts using a magnet, the amount of absorbance is measured (A_t). The pollutant removal efficiency can be calculated using Eq. (1) (Abbasi 2021a, b, 2023a).

$$RE\ (\%\ ) = \frac{A_0 - A_t}{A_0} \times 100 \tag{1}$$

In order to perform statistical analysis, sufficient accuracy should be applied in measuring the amount of responses. Therefore, to ensure this issue, all measurements are repeated three times and the average recorded values are reported. The statistical analysis of the results is done based on analysis of variance using Design-Expert version 7.0.0 software.

Results and discussion

Characterization of synthesized photocatalysts

Figures 1 and 2 show the FTIR analysis of $Fe_3O_4@TiO_2$ and MGO@TiO_2 photocatalysts, respectively. As can be seen, several characteristic peaks have been created, which are attributed to the bonding vibrations of different atoms in the structure of photocatalysts. Considering that the bond
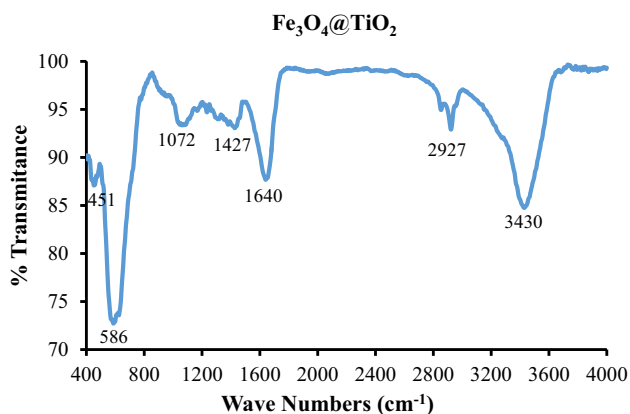

Fig. 1 FTIR spectra of $Fe_3O_4@TiO_2$

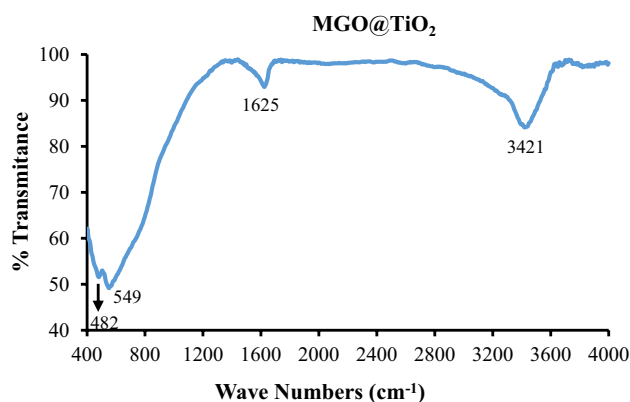**Fig. 2** FTIR spectra of MGO@TiO_2

vibrations between titanium and oxygen atoms (Ti–O) in the structure of TiO_2 nanoparticles are in the range of 430–550 cm^{-1} (Abbasi 2022), therefore, the peak appearing in this range can be attributed to the presence of TiO_2 nanoparticles. In addition to the characteristic peak related to TiO_2 nanoparticles, a characteristic peak is observed at wavelength 586 cm^{-1} (Fig. 1) and wavelength 549 cm^{-1} (Fig. 2). These peaks can be caused by stretching vibrations of iron and oxygen bonds (Fe–O) in Fe_3O_4 nanoparticles (Abareshi et al. 2010). Therefore, the presence of these peaks confirms the presence of magnetic Fe_3O_4 nanoparticles in both synthesized photocatalysts. The vibration of oxygen and hydrogen bonds (H–O) in the hydroxyl functional groups causes a relatively broad peak in the wavelength range of 3400 cm^{-1} (Dastan et al. 2017). As can be seen from Figs. 1 and 2, a broad peak appeared in the same wavelength range in both figures. Therefore, there are hydroxyl functional groups on the surface of both synthesized samples, which increases the stability in aqueous solutions. In both Figs. 1 and 2, the characteristic peak formed in the wavelength range of 1625–1640 cm^{-1} can be attributed to deformative vibration of the bond between titanium and hydroxyl (Ti–OH) stretching (Chougala et al. 2017). The characteristic peak appearing in this range can also be related to the water absorbed on the surface of the photocatalysts. Due to the presence of graphene oxide in the structure of the MGO@TiO_2 photocatalyst, the peak appearing at the wavelength of 1625 cm^{-1} which can be seen in Fig. 2 can be attributed to sp^2-hybridized of C=C (Dastan et al. 2016).

The magnetic hysteresis curves of $Fe_3O_4@TiO_2$ and MGO@TiO_2 photocatalysts are shown in Figs. 3 and 4, respectively. Considering the absence of hysteresis in the presented magnetic cycles of both synthesized photocatalysts, the superparamagnetic property of both synthesized photocatalysts can be confirmed. By exposing the magnetic photocatalysts under a magnetic field, their moments are placed along the applied field. When all moments of
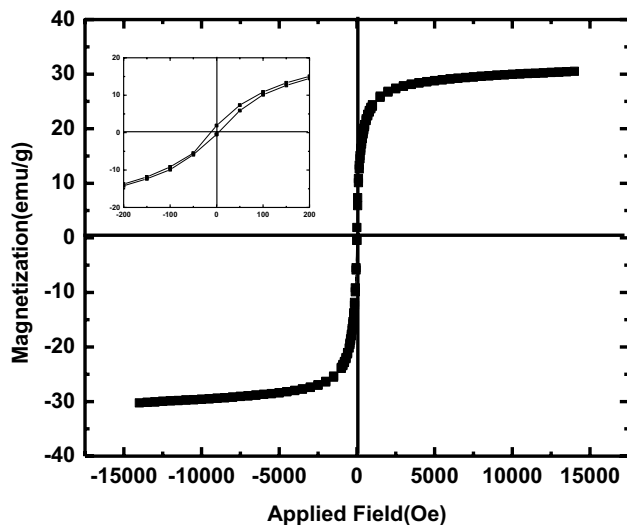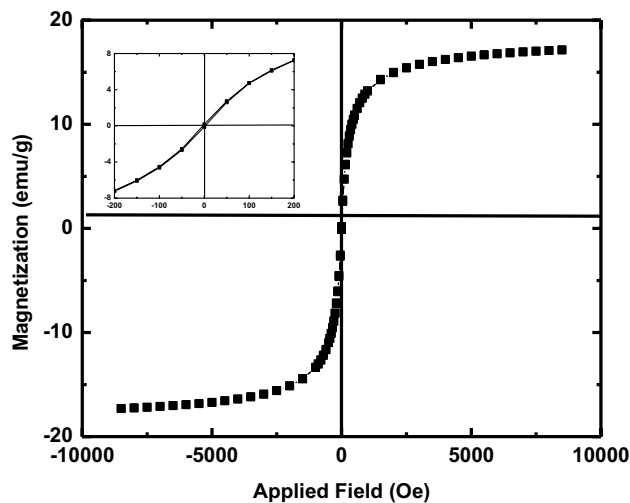
Fig. 3 Magnetization cycle for $Fe_3O_4@TiO_2$

Fig. 4 Magnetization cycle for $MGO@TiO_2$

Fig. 5 The variation of MO removal efficiency with respect to time in the presence of $Fe_3O_4@TiO_2$, influence of photocatalyst's concentration

Fig. 6 The variation of MO removal efficiency with respect to time in the presence of $MGO@TiO_2$, influence of photocatalyst's concentration

photocatalysts are aligned with the magnetic field, the magnetization reaches its highest value, which is considered as saturation magnetization (Ms). The investigation of saturation magnetization of photocatalysts shows that $Fe_3O_4@TiO_2$ and $MGO@TiO_2$ photocatalysts have saturation magnetization equal to 30.5077 emu/g and 17.15 emu/g, respectively. The lower saturation magnetization of the $MGO@TiO_2$ compared to $Fe_3O_4@TiO_2$ can be attributed to the difference in the composition of the two photocatalysts. In fact, due to the presence of more non-magnetic nanoparticles in the structure of the $MGO@TiO_2$ (including titania and graphene oxide) compared to $Fe_3O_4@TiO_2$ (magnetic titania), the degree of saturation magnetization also decreases in the second sample.
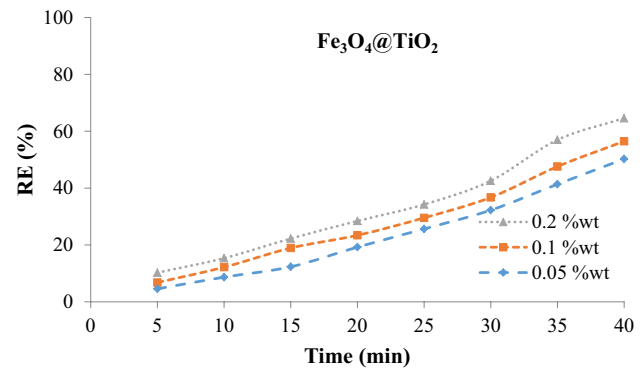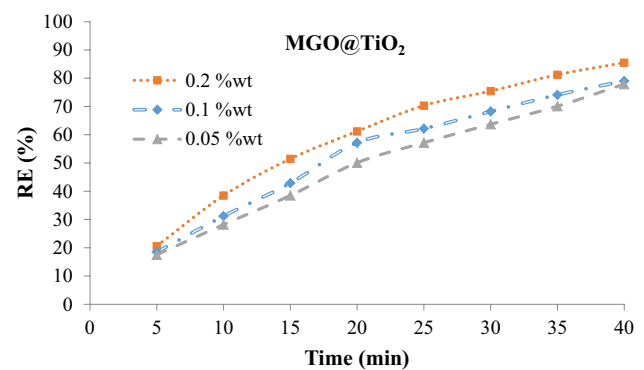
By reversing the magnetic field, it is possible to return the magnetization to the turning point. However, some torques lose the ability to align with the magnetic field and deviate. While other torques remain aligned with the field which is considered as remnant magnetization. The residual magnetization value of the first and second photocatalysts is 1.8965 emu/g and 0.1024 emu/g, respectively. Also, the coercive field value of both photocatalysts is zero. According to the values of residual magnetization and coercive field of these two photocatalysts, the superparamagnetic property of both photocatalysts is confirmed. The obtained results agree with the results of previous reports (Ma et al. 2013).

Removal efficiency investigations

The effect of irradiation time and photocatalyst concentration on the removal efficiency of methyl orange in the presence of $Fe_3O_4@TiO_2$ and $MGO@TiO_2$ as photocatalysts is shown in Figs. 5 and 6, respectively. It is quite clear that the irradiation time of the aqueous suspension containing methyl

orange and photocatalyst has a positive effect on the removal efficiency. In fact, the increasing effect of irradiation time is independent of the type of applied photocatalyst and also its concentration. Therefore, in all concentrations of the photocatalyst, increasing the irradiation time causes a decrease in the concentration of methyl orange and, as a result, an increase in the decomposition efficiency. The increasing effect of irradiation time can be attributed to the produced electron–hole pairs. In fact, when the photocatalysts are exposed to the radiation of the UV light source, considering that the energy of the light source embedded in the photoreactor is more than the band gap energy of the photocatalyst, therefore, the exposure of the photocatalyst to the UV light causes the valence layer electrons to be excited. By stimulating the photocatalyst valence layer electrons, the electrons have the ability to separate from this layer and transfer to the conduction layer (WANG et al. 2009). For each electron that is transferred from the valence layer to the conduction layer, an electron is created in the conduction layer and a hole is created in the valence layer, respectively. The produced electron–hole pairs are the main factor in the decomposition of various organic pollutants. In fact, the generated electrons have the ability to react with dissolved oxygen in the suspension and produce reactive oxygen radicals ($O_2^.$). Also, holes can react with water and form active hydroxyl radicals ($OH^.$) (Abbasi 2023a, b; Abbasi et al. 2022). The created radicals are very active in absorbing all kinds of dye organic pollutants as well as their decomposition. Therefore, with the increase in the number of electron–hole pairs produced, which is caused by the increase in the irradiation time, the

decomposition rate of methyl orange also increases significantly. The mechanism of photocatalytic reactions is shown schematically in Fig. 7. In addition to the significant effect of time on the decomposition of methyl orange, the significant role of the concentration of $Fe_3O_4@TiO_2$ and $MGO@TiO_2$ can be deduced in Figs. 5 and 6, respectively. Changing the concentration of the photocatalyst in the range of 0.05% by weight to 0.2% by weight causes a decrease in the concentration of the pollutant and an increase in the decomposition efficiency, which can be attributed to the increase in the effective contact surface of the photocatalyst with light radiation. In fact, increasing the contact surface leads to an increase in the number of excited electrons that have the ability to transfer from the valence layer to the conduction layer. Therefore, it dramatically increases the number of electron–hole pairs and subsequently increases the number of active oxidizing radicals, including hydroxyl and oxygen radicals (Roozban et al. 2017a, b).

The comparison of the changes in the removal efficiency of methyl orange using $Fe_3O_4@TiO_2$ and $MGO@TiO_2$ at different weight fraction can be seen in Fig. 8. According to the results, it can be seen that the removal efficiency of methyl orange in the presence of $MGO@TiO_2$ is much higher than the $Fe_3O_4@TiO_2$. The higher photocatalytic activity of $MGO@TiO_2$ can be related to the presence of graphene oxide sheets in the photocatalyst structure. The presence of graphene oxide reduces the accumulation of TiO_2 nanoparticles, and this leads to the uniform distribution of single nanoparticles on the surface of graphene oxide. Considering that the amount of agglomeration of TiO_2 nanoparticles in the
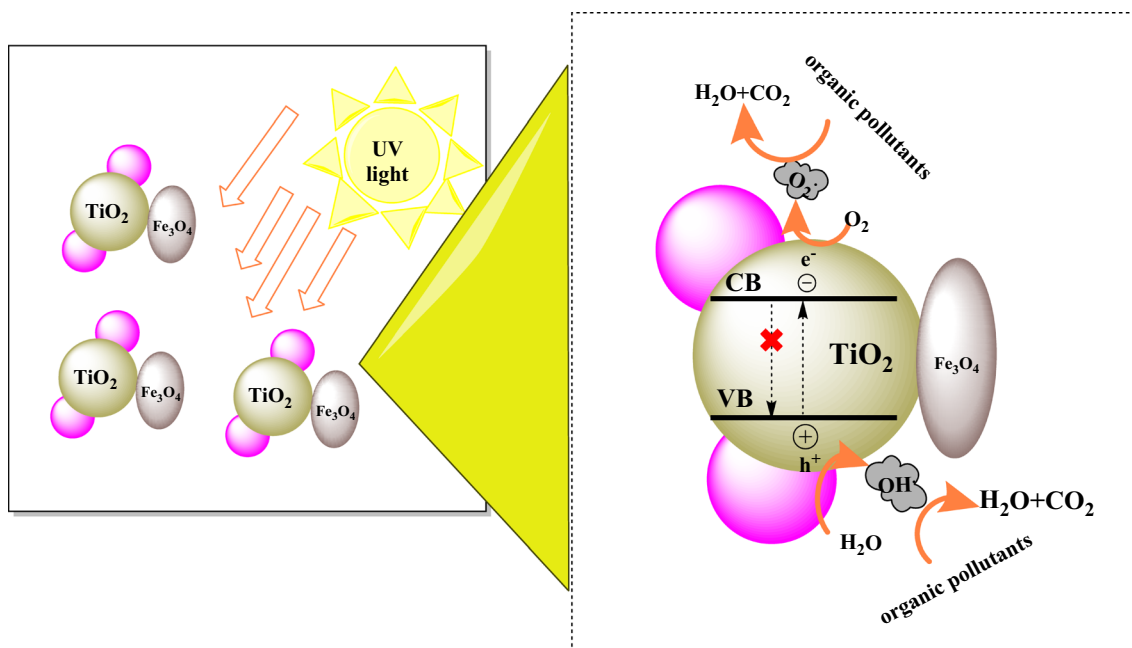
Fig. 7 Schematic of photocatalytic reactions for organic pollutants decomposition
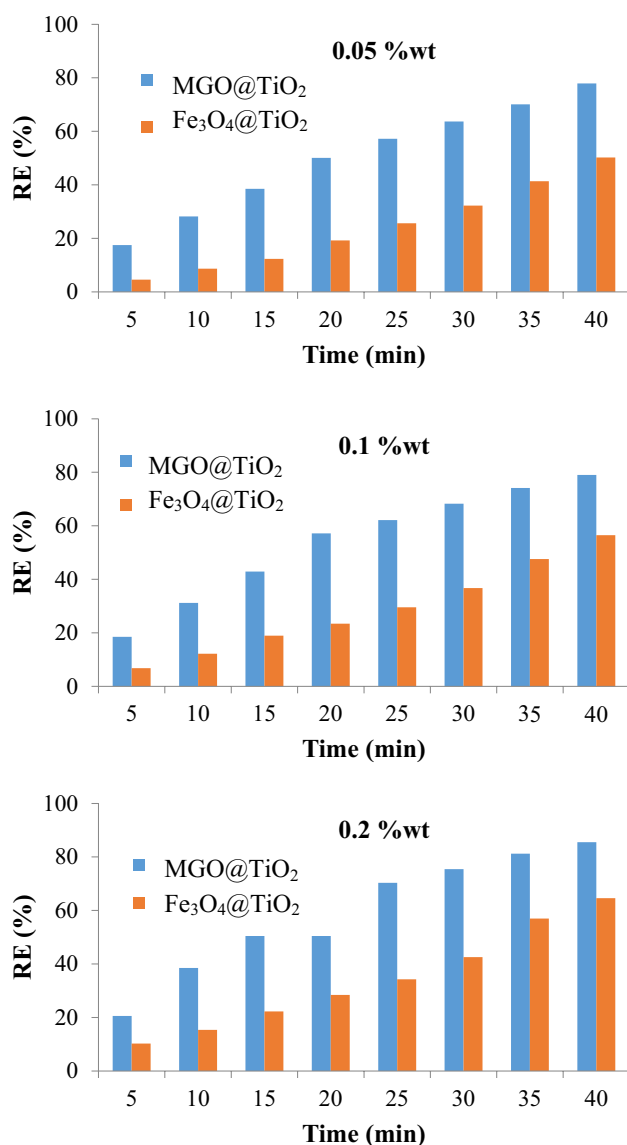
Fig. 8 Comparison the photocatalytic activity of $Fe_3O_4@TiO_2$ and $MGO@TiO_2$ to degradation of methyl orange at different weigh fraction of photocatalyst

$MGO@TiO_2$ is much less than the $Fe_3O_4@TiO_2$, therefore, the active surface of the photocatalyst which is exposed to the radiation of the light source as well as methyl orange has

a significant increase. This causes a significant increase in the amount of oxidizing radicals as well as the photocatalytic activity of the $MGO@TiO_2$ compared to the $Fe_3O_4@TiO_2$.

Statistical investigations

Statistical studies are used to analyze and confirm experimental results. In order to investigate pollutant decomposition in the presence of different photocatalysts as well as the effect of operating parameters, the data of the analysis of variance (ANOVA) table provide useful information regarding the changes in the removal rate of methyl orange. The analysis of variance table of methyl orange decomposition using $Fe_3O_4@TiO_2$ and $MGO@TiO_2$ is presented in Tables 1 and 2, respectively. The results presented in these two tables are based on a confidence level of 5%. Therefore, if any of the operational parameters such as irradiation time and photocatalyst concentration or mutual interaction between the main factors have a p value lower than the confidence level, they are considered as an important and significant factor (Abbasi et al. 2020; Abbasi et al. 2017a, b). According to the *p* value of both main single factors presented in Tables 1 and 2, it can be concluded that the irradiation time and the concentration of both photocatalysts have a significant effect on the removal of methyl orange. While the interaction of time and concentration does not show the same behavior in the removal of methyl orange using $Fe_3O_4@TiO_2$ and $MGO@TiO_2$. Another significant statistical proctor is *F*-value. The *F*-value of each parameter indicates its importance and influence on the response (Ekrami-Kakhki et al. 2018). By comparing the *F*-values of the independent factors presented in Tables 1 and 2, it can be seen that the *F*-value of the irradiation time is much higher than the concentration of the photocatalyst. This shows that the effect of irradiation time on the removal of methyl orange using both photocatalysts is much higher than the concentration. The proposed model in statistical analysis has the ability to estimate the changes in methyl orange removal efficiency by changing significant factors. The suggested statistical models using $Fe_3O_4@TiO_2$ and $MGO@TiO_2$ have *P*-value less than 0.05. Therefore, the adequacy of the models is acceptable, and it can be expected that the values estimated by these two models are consistent with the laboratory values. It should be

Table 1 Analysis of variance for MO decomposition in the presence of $Fe_3O_4@TiO_2$

Source	Sum of square	Df	Mean squares	*F*-value	*p* value	% contribution	
Model	20,753.18	23	902.31	292.85	<0.0001	–	Significant
A (Time)	19,407.33	7	2772.48	899.81	<0.0001	92.85	Significant
B (Weight fraction)	1210.71	2	605.36	196.47	<0.0001	5.79	Significant
A-B	135.14	14	9.65	3.13	0.0016	0.65	Significant
Pure error	147.90	48	3.08	–	–	0.71	–
Total	20,901.07	71	–	–	–	–	–

Table 2 Analysis of variance for MO decomposition in the presence of MGO@TiO$_2$

Source	Sum of square	Df	Mean squares	F-value	P-value	% contribution	
Model	30,619.63	9	3402.18	432.18	<0.0001	–	Significant
A (Time)	29,354.90	7	4193.56	532.70	<0.0001	94.37	Significant
B (Weight fraction)	1264.73	2	632.36	80.33	<0.0001	4.04	Significant
A-B	125.21	14	8.94	1.18	0.3183	0.4	Not significant
Pure error	362.87	48	7.56	–	–	1.17	–
Total	31,107.71	71	–	–	–	–	–

kept in mind that due to the insignificance of the interaction of the main factors (A-B) in Table 2, the proposed model by the MGO@TiO$_2$ does not have an interaction parameter. The percentage of participation of the main factors in the proposed models can be seen in Tables 1 and 2. As it can be seen, the irradiation time has the most contribution in the presented models, which is completely consistent with the results of the F-value.

Model adequacy study based on graphical statistical analysis

According to the results of statistical analysis and analysis of variance tables, it is observed that the changes in the removal efficiency of methyl orange can be predicted with respect to the irradiation time, photocatalyst weight fraction and also the interaction between them. Therefore, in order to ensure the results of the values estimated by the proposed models, it is important to check the adequacy of the models. One of the methods of checking the adequacy of the presented models is the graphical analysis method. In this method, the correctness of the assumptions made for analysis of variance should be examined. The most important assumption made for analysis of variance is normal distribution and independence of residuals (Namvar-Mahboub and Pakizeh 2014). The normal distribution curve of methyl orange removal efficiency using the Fe$_3$O$_4$@TiO$_2$ and MGO@TiO$_2$ is shown in Figs. 9 and 10, respectively. As can be seen, the changes of the normal probability with respect to the studentized residuals are on a straight line, and the existence of any relationship, including the S-shape, is negated. Therefore, we can confidently confirm the normal distribution of the error, which can confirm the adequacy of the presented models.

Figures 11 and 12 show the outlier T plot for presented modes using Fe$_3$O$_4$@TiO$_2$ and MGO@TiO$_2$, respectively. According to these two Figures, it is possible to determine the deviation between the residuals or the error with the removal efficiency. What is evident is that all the experimental data in Fig. 11 are within the allowed range and only one of the design data in Fig. 12 is outside the range. Placing this point outside the range can be due to measurement error during the test. Due to the small number of these points, it
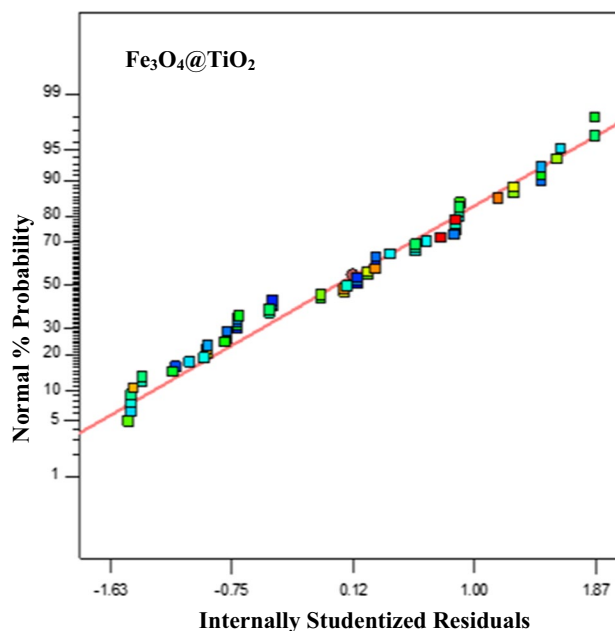
Fig. 9 Normal distribution curve of residuals for removal efficiency using Fe$_3$O$_4$@TiO$_2$

can be ignored. Therefore, it is clear that all the points used in the statistical analysis and leading to the creation of a proposed model have had the necessary and sufficient accuracy. Therefore, the models that have been proposed based on statistical analysis to estimate the removal efficiency of methyl orange are adequate.

Conclusions

A magnetic nanocomposite composed of graphene oxide, TiO$_2$ nanoparticles, and Fe$_3$O$_4$ nanoparticles is synthesized to investigate the efficiency of methyl orange decomposition as an organic pollutant, and its photocatalytic activity is compared with the photocatalyst without graphene oxide. Examining the results showed that the presence of graphene oxide in the photocatalyst structure significantly increases the decomposition
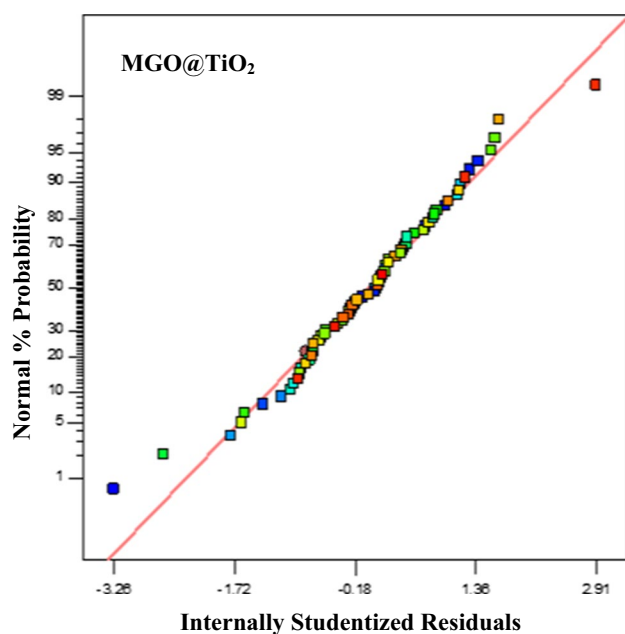
Fig. 10 Normal distribution curve of residuals for removal efficiency using MGO@TiO$_2$
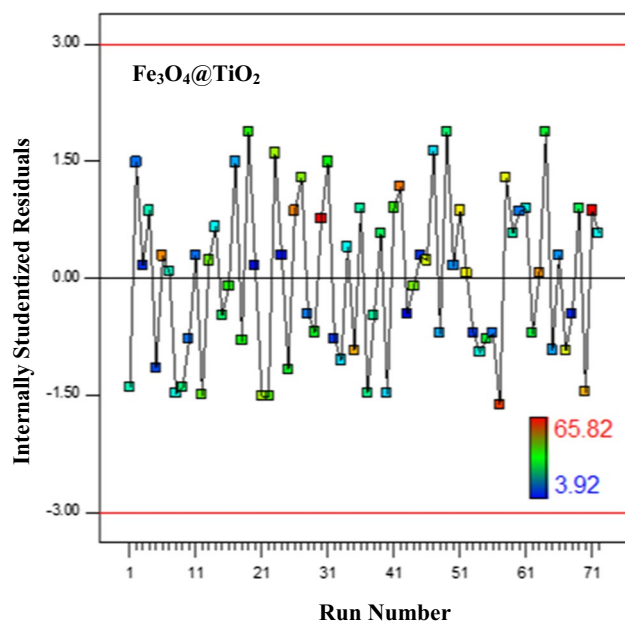
Fig. 11 The outlier T plot for Fe$_3$O$_4$@TiO$_2$ model

efficiency, and the main reason for this increase is the role of graphene oxide in the uniform distribution of photocatalytic nanoparticles and preventing their agglomeration during the synthesis process. Statistical studies of the results based on analysis of variance showed that the irradiation time and the concentration of magnetic photocatalysts have a significant effect on the removal
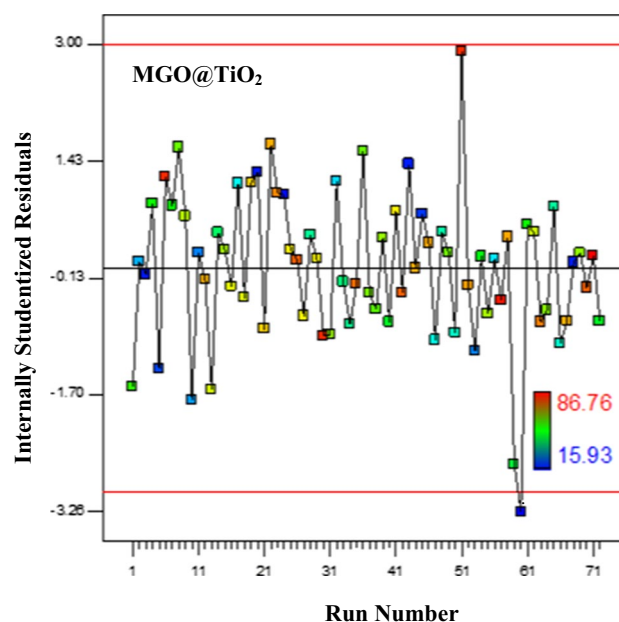
Fig. 12 The outlier T plot for MGO@TiO$_2$ model

efficiency of methyl orange. According to the confirmation of the adequacy of the proposed statistical model, the changes of photocatalytic activity can be estimated with high accuracy in relation to the irradiation time and photocatalyst concentration.

Data availability The authors confirm that the data supporting the findings of this study are available within the article.

Declarations

Conflict of interest The authors declare no competing interests.

Compliance with ethical standards I promise that I have followed all the ethical principles.

References

Abareshi M, Goharshadi EK, Zebarjad SM, Fadafan HK, Youssefi A (2010) Fabrication, characterizationandmeasurementof thermal conductivity of F_e3_O4 nanofluids. J Magn Magn Mater 322:3895–3901

Abbasi S (2018) Investigation of the enhancement and optimization of the photocatalytic activity of modified TiO2 nanoparticles with SnO2 nanoparticles using statistical method. Mater Res Express 5:066302

Abbasi S (2019) Photocatalytic activity study of coated anatase-rutile titania nanoparticles with nanocrystalline tin dioxide based on the statistical analysis. Environ Monit Assess 191:206

Abbasi S (2020) Adsorption of dye organic pollutant using magnetic ZnO embedded on the surface of graphene oxide. J Inorg Organomet Polym Mater 30:1924–1934

Abbasi S (2021a) Improvement of photocatalytic decomposition of methyl orange by modified MWCNTs, prediction of degradation rate using statistical models. J Mater Sci Mater Electron 32:14137–14148

Abbasi S (2021b) Response surface methodology for photo degradation of methyl orange using magnetic nanocomposites containing zinc oxide. J Cluster Sci 32:805–812

Abbasi S (2022) The degradation rate study of methyl orange using MWCNTs@ TiO2 as photocatalyst, application of statistical analysis based on fisher's F distribution. J Cluster Sci 33:593–602

Abbasi S (2023a) Magnetic photocatalysts based on graphene oxide: synthesis, characterization, application in advanced oxidation processes and response surface analysis. Appl Water Sci 13:1–11

Abbasi S (2023b) Studying the destruction of pollutant in the presence of photocatalysts based on MWCNTs with controlled values of TiO_2 nanoparticles. Appl Water Sci 4:100

Abbasi S, Hasanpour M (2017) The effect of pH on the photocatalytic degradation of methyl orange using decorated ZnO nanoparticles with SnO_2 nanoparticles. J Mater Sci Mater Electron 28:1307–1314

Abbasi S, Zebarjad SM, Baghban SHN, Youssefi A (2015) Synthesis of TiO2 nanoparticles and decorated multiwalled carbon nanotubes with various content of rutile titania. Synth React Inorg, Met-Org, Nano-Met Chem 45:1539–1548

Abbasi S, Ekrami-Kakhki M-S, Tahari M (2017a) Modeling and predicting the photodecomposition of methylene blue via ZnO–SnO 2 hybrids using design of experiments (DOE). J Mater Sci Mater Electron 28:15306–15312

Abbasi S, Hasanpour M, Ekrami-Kakhki M-S (2017b) Removal efficiency optimization of organic pollutant (methylene blue) with modified multi-walled carbon nanotubes using design of experiments (DOE). J Mater Sci Mater Electron 28:9900–9910

Abbasi S, Ahmadpoor F, Imani M, Ekrami-Kakhki M-S (2020) Synthesis of magnetic Fe3O4@ ZnO@ graphene oxide nanocomposite for photodegradation of organic dye pollutant. Int J Environ Anal Chem 100:225–240

Abbasi S, Dastan D, Ţălu Ş, Tahir M, Elias M, et al. (2022) Evaluation of the dependence of methyl orange organic pollutant removal rate on the amount of titanium dioxide nanoparticles in MWCNTs-TiO_2 photocatalyst using statistical methods and Duncan's multiple range test. Int J Environ Anal Chem 1–15

Abdel-Messih MF, Ahmed MA, El-Sayed AS (2013) Photocatalytic decolorization of rhodamine B dye using novel mesoporous SnO_2–TiO_2 nano mixed oxides prepared by sol–gel method. J Photochem Photobiol, A 260:1–8

Benjwal P, Kumar M, Chamoli P, Kar KK (2015) Enhanced photocatalytic degradation of methylene blue and adsorption of arsenic(iii) by reduced graphene oxide (rGO)–metal oxide (TiO_2/Fe_3O_4) based nanocomposites. RSC Adv 5:73249–73260

Chougala LS, Yatnatti MS, Linganagoudar RK, Kamble RR, Kadadevarmath JS (2017) A simple approach on synthesis of TiO_2 nanoparticles and its application in dye sensitized solar cells. J Nano Electron Phys 9:04005–04010

Dastan D, Panahi SL, Chaure NB (2016) Characterization of titania thin films grown by dip-coating technique. J Mater Sci Mater Electron 27:12291–12296

Dastan D, Chaure N, Kartha M (2017) Surfactants assisted solvothermal derived titania nanoparticles: synthesis and simulation. J Mater Sci Mater Electron 28:7784–7796

Ekrami-Kakhki M-S, Abbasi S, Farzaneh N (2018) Design of experiments methodology to investigate methanol electrooxidation on Pt nanoparticles supported novel functionalized reduced graphene oxide. Anal Bioanal Electrochem 10:1548–1561

Fan H, Yi G, Zhang X, Xing B, Zhang C et al (2021) Facile synthesis of uniformly loaded Fe_3O_4–TiO_2/RGO ternary hybrids for enhanced photocatalytic activities. Opt Mater 111:110582

Gan L, Li H, Chen L, Xu L, Liu J et al (2018) Graphene oxide incorporated alginate hydrogel beads for the removal of various organic dyes and bisphenol A in water. Colloid Polym Sci 296:607–615

Gao P, Sun DD (2014) Hierarchical sulfonated graphene oxide–TiO_2 composites forhighly efficient hydrogen production with a wide pH range. Appl CatalB-Environ 147:888–896

Ghaderi A, Abbasi S, Farahbod F (2018) Synthesis, characterization and photocatalytic performance of modified ZnO nanoparticles with SnO2 nanoparticles. Mater Res Express 5:065908

Kim SP, Choi MY, Choi HC (2015) Characterization and photocatalytic performance of SnO2-CNTnanocomposites. Appl Surf Sci 357:302–308

Ma P, Jiang W, Wang F, Li F, Shen P et al (2013) Synthesis and photocatalytic property of Fe_3O_4@TiO_2 core/shell nanoparticles supported by reduced graphene oxide sheets. J Alloy Compd 578:501–506

Namvar-Mahboub M, Pakizeh M (2014) Optimization of preparation conditions of polyamide thin film composite membrane for organic solvent nanofiltration. Korean J Chem Eng 31:327–337

Reddy DA, Ma R, Kim TK (2015) Efficient photocatalytic degradation of methylene blue by heterostructured ZnO–RGO/RuO_2 nanocomposite under the simulated sunlight irradiation. Ceram Int 41:6999–7009

Roozban N, Abbasi S, Ghazizadeh M (2017a) The experimental and statistical investigation of the photo degradation of methyl orange using modified MWCNTs with different amount of ZnO nanoparticles. J Mater Sci Mater Electron 28:7343–7352

Roozban N, Abbasi S, Ghazizadeh M (2017b) Statistical analysis of the photocatalytic activity of decorated multi-walled carbon nanotubes with ZnO nanoparticles. J Mater Sci Mater Electron 28:6047–6055

Tao L, Dastan D, Wang W, Poldorn P, Meng X et al (2023) Metal-decorated InN monolayer senses N_2 against CO_2. ACS Appl Mater Interfaces 15:12534–12544

Wang X, Yao S, Li X (2009) Sol-gel preparation of CNT/ZnO nanocomposite and its photocatalytic property. Chin J Chem 27:1317–1320

Yuan NY, Ma FF, Fan Y, Liu YB, Ding JN (2012) High conductive ethylene vinyl acetate composites filled with reduced graphene oxide and polyaniline. Compos Part A 43:2183–2188

Zhu G, Wang H, Yang G, Chen L, Guo P et al (2015) A facile synthesis of ZnO/CNTs hierarchical mircosphere composites with enhanced photocatalytic degradation of methylene blue. RSC Adv 5:72476–72481